Geochemical Perspectives Letters

Determining subduction-zone fluid composition using a tourmaline mineral probe

V.J. van Hinsberg[1*], G. Franz[2], B.J. Wood[3]

OPEN ACCESS

doi: 10.7185/geochemlet.1719

Abstract

Subduction zones are the sites where crustal materials are recycled into the mantle. In response to increasing pressures and temperatures during this process, hydrated minerals break down and release solute-bearing fluids and, above ~750 °C, form hydrous melts. Magmas generated by interaction of these melts and fluids with the mantle have a characteristic arc elemental signature. Here, a zoned refractory tourmaline grain, formed during Alpine subduction and uplift, was used to reconstruct the compositions of the fluids involved in element transfer. The reconstructed compositions confirm that slab-released fluids carry the arc-signature, and suggest that mineral–fluid element partitioning controls their compositions. However, these fluids are calculated to be dilute. To reconcile this with higher element-to-water ratios required for arc magmas, a two-stage arc-magma genesis model is favoured where fluids imprint their compositional signature progressively on a slab mélange that is subsequently transferred to, and interacts with the mantle to generate arc magmas.

Received 2 September 2016 | Accepted 6 March 2017 | Published 28 March 2017

Introduction

The principal material fluxes from the surface into the deep Earth take place at subduction zones. Models of terrestrial element cycling hinge on accurate estimates of these fluxes and of the recycling of material by fluids and melts from the dehydrating slab in the "subduction factory" (Tatsumi, 2005). Estimates of element release from the slab, and hence constraints on the net flux through subduction zones, are derived from three main sources; (i) the compositional signatures of arc magmas (*e.g.,* Elliott *et al.*, 1997), which are Nb-Ta depleted and enriched in Li, B, Sr, Ba and Pb compared to mid-ocean ridge basalts (MORB);

1. Department of Earth and Planetary Sciences, McGill University, Montreal, Quebec, Canada
* Corresponding author (email: V.J.vanHinsberg@gmx.net)
2. Department of Applied Geosciences, Technical University Berlin, Berlin, Germany
3. Department of Earth Sciences, University of Oxford, United Kingdom

(ii) experimentally-determined element partitioning between subduction-zone solids and liquids (*e.g.,* Keppler, 1996; Kessel *et al.*, 2005; Hermann *et al.*, 2006; Spandler *et al.*, 2007; Tsay *et al.* 2017); and (iii) element mass-balance on subducted rock lithologies (*e.g.,* Bebout *et al.*, 1999; Spandler *et al.*, 2003, 2004). Methods (i) and (iii) provide information on mass transfer from subducting lithologies into the region of melt generation, but no detail on element concentrations in fluids and melt, or total fluxes. Moreover, (iii) depends on the presence of accessory phases (see Klimm *et al.*, 2008; Hermann and Rubatto, 2009), as these phases can be the dominant repository of certain trace elements in the bulk rock. This fact makes the method critically dependent on preservation of these phases, as well as their representative sampling in bulk-rock studies. Method (ii) provides concentration information, and flux estimates when combined with models of release of volatiles (*e.g.,* Spandler *et al.*, 2003; Connolly, 2005), but only under model-dependent conditions of temperature, pressure, mineralogy and bulk composition. What is needed is a more direct record of subduction-zone fluid composition.

Here, well-preserved subduction-zone minerals (tourmaline, titanite and phengite) are used to quantitatively reconstruct the compositions of the fluids from which they grew by combining mineral compositions with mineral–fluid element partition coefficients (*cf.* Keppler, 1996). If D-values are known for the physico-chemical conditions of growth, absolute element concentrations in the fluid result. This approach avoids any assumption of the presence of accessory phases, but rather allows for their presence to be tested. Furthermore, minerals can simultaneously yield *P–T* conditions and age of growth that can be combined directly with reconstructed fluid compositions into a comprehensive and internally consistent database of the *P–T–X-t* evolution of a subduction zone.

Tourmaline as a Mineral Probe

A tourmaline grain from the Tauern Window Eclogite Zone (Austrian Alps) is the principal probe of fluid compositions in this study. The mineral tourmaline has exceptional *P–T* stability that covers subduction-zone conditions (Fig. S-1); its crystal-chemistry allows it to incorporate a diversity of (trace) elements; and it displays negligible volume-diffusional re-equilibration (*e.g.,* Henry and Dutrow, 1996; van Hinsberg *et al.*, 2011a,b). These features allow tourmaline to record its host environment composition throughout subduction and to preserve it for later interrogation. Tourmaline's presence is dictated by the availability of boron, rather than by *P–T* conditions. At low grades, B dominantly resides in sheet silicates (Leeman and Sisson, 1996) and is released during prograde metamorphism in discontinuous reactions resulting in punctuated nucleation and growth, and in continuous reactions producing gradual growth. Owing to negligible diffusive re-equilibration, this growth is expressed as growth zones.

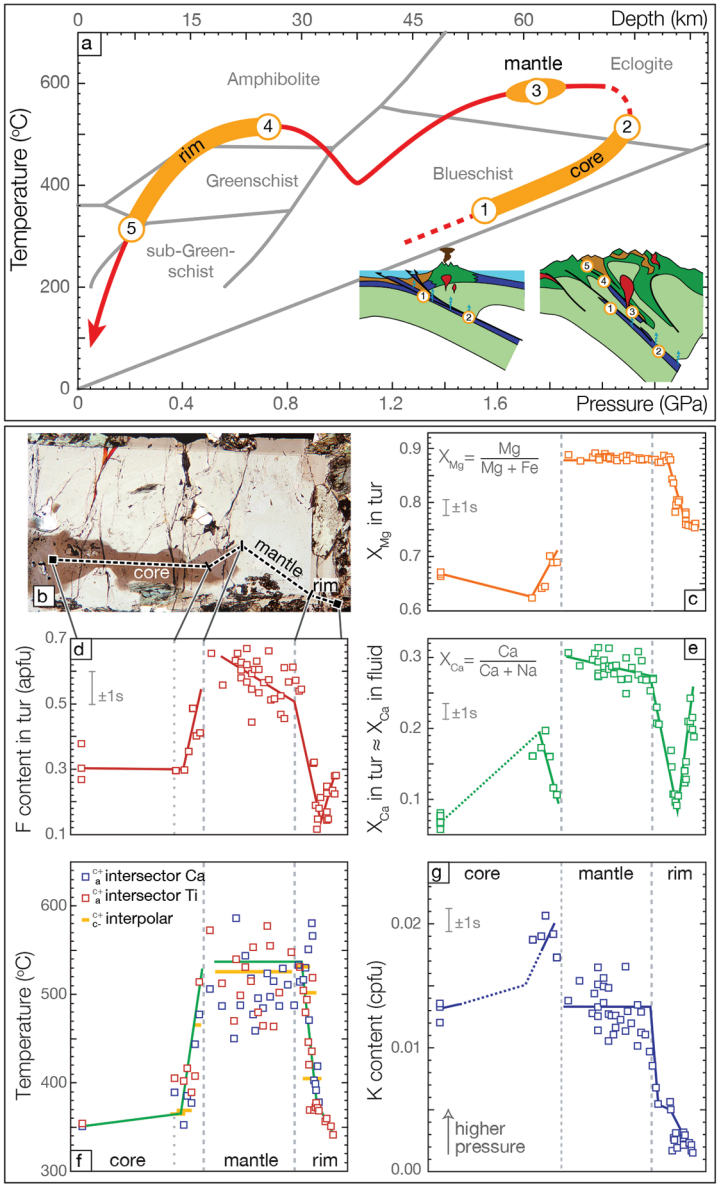

Figure 1 Reading the Tauern tourmaline record. **(a)** Tauern Eclogite Zone *P–T* path (Zimmermann *et al.*, 1994) with conditions recorded by tourmaline growth zones shown. Inset cartoons locate these in a schematic subduction-zone cross-section. **(b)** PPL image of the tourmaline transect. **(c)** X_{Mg} sharply defines the tourmaline growth zones. **(d)** F-content in tourmaline, >0.5 apfu F in the outer core and mantle. **(e)** X_{Ca} of tourmaline, which tracks the X_{Ca} in the coexisting fluid (von Goerne *et al.*, 2011). **(f)** Temperature transect across the tourmaline grain calculated from inter-sector and inter-polar thermometry. **(g)** Tourmaline K-content, which acts as a qualitative barometer. Uncertainties shown are the typical 1s analytical precision.

The Tauern tourmaline grain occurs in a meta-sedimentary retrogressed eclogite that preserves relics of a garnet–omphacite–phengite–titanite eclogite paragenesis, overprinted by an amphibolite-facies amphibole–plagioclase–epidote–carbonate paragenesis (Fig. S-2a). Peak conditions for this unit have been estimated at 630 °C and 2.5 GPa (*e.g.*, Selverstone *et al.*, 1992; Hoschek, 2007). There is no evidence for partial melting and tourmaline is interpreted to have formed from aqueous fluid throughout its growth history. Tourmaline is a minor accessory phase in these rocks, and is therefore unable to exert control on element concentrations in the fluid. Rather, it acts as a passive recorder of its environment.

Detailed petrographic examination reveals a zoned brown core, a blue-green mantle, and a strongly zoned outer rim (see the Supplementary Information for more details). Hourglass sector-zoning is present (Fig. S-2b), indicating that growth compositions have been preserved (van Hinsberg *et al.*, 2006). Inter-sector thermometry (van Hinsberg and Schumacher, 2007), combined with qualitative K-barometry and inclusion mineralogy suggests growth of the tourmaline core during prograde subduction and its associated progressive internal B-release, formation of the mantle zone following detachment from the subducting slab from external fluids that were released in deeper slab devolatilisation, and rim growth during retrogression that records the orogenic uplift of the Eclogite Zone (Fig. 1a). This single tourmaline grain thus chronicles the subduction to uplift history, and can provide information on the associated fluids at multiple stages along this path.

Tourmaline Composition and Fluid Reconstruction

Compositions of individual tourmaline growth zones and mineral inclusions were determined by EMP (major elements) and LA-ICP-MS (trace elements). Tourmaline compositions are dominated by the dravite end-member with lesser schorl, uvite and foitite, have variable X_{Ca} and X_{Mg}, and high F contents in core and mantle (Fig. 1, Table S-1). Tourmaline and mineral inclusion compositions constrain growth to be from an acidic aqueous solution with Na concentrations from 0.45 to 0.75 mol L^{-1}, variable X_{Ca} and an F-content between 2 and 1400 ppmm (Supplementary Information). Trace element concentrations in tourmaline are low, from tens of ppmm for the LILE to ppbm for the HFSE (Table S-3).

Tourmaline–fluid trace element partition coefficients, required to convert tourmaline compositions to those of their formation fluids, have not been determined experimentally and were therefore estimated (see Supplementary

Information for details and discussion). As a result, absolute concentrations in the fluid calculated from tourmaline are interpreted to have an associated uncertainty of an order of magnitude. However, element ratios, patterns and the overall elemental signature are robust. A further confirmation of reconstructed fluid compositions is the good agreement between the fluid composition reconstructed from the tourmaline mantle, and the same fluid reconstructed from phengite and titanite inclusions within this growth zone (Tables S-2, S-3).

Controls on Fluid Composition

The high-*P* Tauern subduction-zone fluids, reconstructed from tourmaline, phengite and titanite, are dilute aqueous solutions with <0.75 mol L^{-1} Na and total trace element concentrations <500 ppmm (Fig. 2a). Titanium concentrations suggest saturation in rutile when experimental solubilities (Manning *et al.*, 2008; Rapp *et al.*, 2010; Tsay *et al.*, 2017) are extrapolated to Tauern conditions, consistent with the presence of rutile inclusions in tourmaline's core and mantle. In contrast, fluid REE concentrations are at a median level of only tens of ppbm (Fig. 2a), which is at least 2 orders of magnitude below that required for saturation in the common REE-minerals (Tropper *et al.*, 2011). This level is consistent with REE concentrations in eclogite-fluid experiments with allanitic zoisite (Tsay *et al.*, 2017), where mineral–fluid partitioning, rather than mineral solubility would control REE concentrations.

Fluid compositions reconstructed from well-preserved high-*P* minerals from the Dora Maira, Syros and New Caledonia palaeo-subduction zones using a similar methodology overlap with those reconstructed for the Tauern Eclogite Zone (Fig. 2a). Absolute concentrations vary by 2–3 orders of magnitude, but elemental patterns are consistent, and similarly suggest rutile-saturated, but REE-phase-undersaturated conditions. Hence, Ti concentrations will be controlled by solubility and are therefore independent of bulk-rock composition and mineral paragenesis until the saturating phase is exhausted (see Klimm *et al.*, 2008). However, for elements controlled by partitioning, such as the REE, differences in slab bulk-rock composition will impart differences in absolute element content of slab-derived fluids. Elemental patterns will persist, assuming no changes in major mineral paragenesis, as is indeed observed (Fig. 2a). Hence, arc magmas will share a characteristic element signature, but absolute concentrations can vary, even on a local scale, depending on the composition and mineralogy of the material that enters the trench.

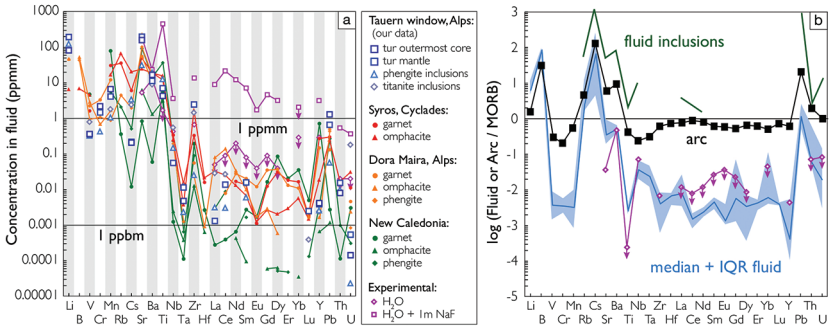

Figure 2 (a) Element concentrations in fluids reconstructed from the Tauern tourmaline outer core and mantle and its mineral inclusions (blue symbols), and eclogite minerals from other subduction-zone terrains show a consistent pattern. **(b)** MORB-normalised concentrations for average arc magma parallel those of subduction-zone fluids supporting a genetic link. See the Supplementary Information for data sources and calculation method. Uncertainties are given as the Interquartile Range (IQR) and maximum estimates marked with an arrow.

Arc Volcanic Compositional Signature

To evaluate the resulting fluid compositions, these are compared in a typical arc-magma plot of $^{Ba}/_{Th}$ vs. $^{La}/_{Sm}$ (Fig. 3). $^{La}/_{Sm}$ is controlled by residual garnet in the slab and high values signify a meta-sedimentary input (*e.g.*, Elliott *et al.*, 1997), whereas $^{Ba}/_{Th}$ indicates fluid involvement, given the contrasting fluid mobility of Ba and Th (*e.g.*, Keppler, 1996; Elliott *et al.*, 1997). Tourmaline-reconstructed fluids show the high $^{Ba}/_{Th}$ at low $^{La}/_{Sm}$ signature expected for subduction-zone fluids. This is moreover most distinct for the outermost core and mantle zones, which are interpreted to record the fluid released in slab devolatilisation and that which flushes the subduction channel, respectively. The latter is modified en-route to enrich fluid-compatible Ba over incompatible Th, consistent with models for subduction-zone fluids (Manning, 2004). Fluids reconstructed from phengite and titanite inclusions in the mantle zone are within error of those derived from tourmaline. $^{Ba}/_{Th}$ values are lowest for the orogenic uplift part of the history, and suggest that a high $^{Ba}/_{Th}$ ratio is characteristic for slab-derived fluids.

Normalised to MORB, the element patterns of the reconstructed fluids, as well as those of fluid inclusions in subduction-zone rocks (*e.g.*, Scambelluri *et al.*, 2001) parallel that of average primitive arc magma; elevated in large-ion lithophile elements while depleted in V, Cr, and Ti (Fig. 2b). This shows that addition of these slab-derived fluids could confer the arc-characteristic element signature, as was concluded for $^{Ba}/_{Th}$.

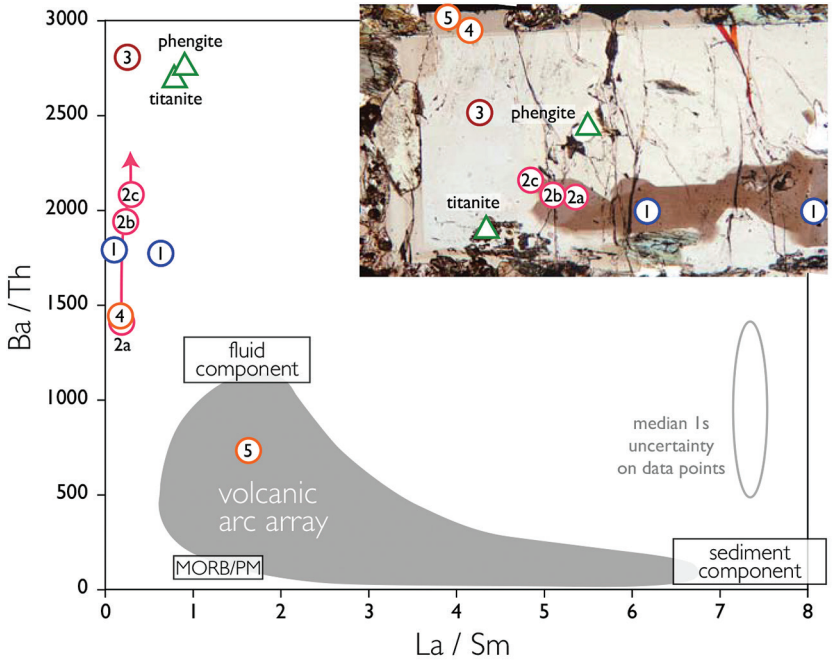

Figure 3 Fluid compositions reconstructed from tourmaline (circles) and its mineral inclusions (triangles), show a consistent, high $^{Ba}/_{Th}$ at low $^{La}/_{Sm}$ signature. Addition of this fluid to the arc-magmatism source region can explain the trend to elevated $^{Ba}/_{Th}$ compared to mid-ocean ridge basalt (MORB) and primitive mantle (PM).

Material Transfer from the Slab to Mantle

A fluid to primitive mantle ratio of 10:3 is required to produce the observed range of $^{Ba}/_{Th}$ in arc magmas. Such high fluid-to-rock ratios are incompatible with the common conceptual model of arc magmatism where mantle is metasomatised by fluids, and subsequently partially molten, to initiate magmatism. Even when fully hydrated, the mantle cannot accommodate more than ~10 wt. % H_2O. Moreover, arc-magmas are incompatible with the compositional dilution that high fluid-rock ratios impart. MORB-normalised fluid compositions (Fig. 2b) are also incompatible with a model of simple fluid addition to the mantle, with reconstructed concentrations of Sr and Ba, for example, unable to lead to the observed enrichment in arc magmas. This suggests a decoupling of water and its solutes during arc magma genesis.

Rather than batch fluid transfer to the mantle, we envision channelling of fluids along the slab interface mélange at high fluid-to-rock ratios. The arc-signature is indeed observed in palaeo-subduction mélanges (Marschall and Schumacher, 2012), and the compositional range therein is in agreement with a progressive, and locally variable imprint of this signature by fluids flushing the mélange. Diapirism of this mélange into the mantle can subsequently transfer the compositional signature to the source region of arc magmas (*cf.* Marschall and Schumacher, 2012 and references therein).

Conclusions

Reconstruction of subduction-zone fluid compositions from eclogite minerals is a powerful method that allows absolute element concentrations in these fluids to be constrained when partition coefficients for the relevant *P–T–X* conditions are known. Tourmaline-reconstructed subduction-zone fluid compositions show that fluid-induced selective element release from the subducting slab can imprint the compositional signature characteristic of arc magmas. The compositions of these fluids appear controlled by mineral-fluid partitioning, except for Ti, and subduction-zone fluids are therefore expected to have variable compositions, but share a common elemental signature. Conversion of these fluid compositions into a net element flux in subduction zones is still imprecise, not least because our data indicate that a simple batch model of element transfer from slab to mantle and crust is untenable. Fluids instead likely migrate along the slab interface and progressively redistribute elements as recorded in refractory minerals.

Acknowledgements

VvH acknowledges financial support from the European Union Seventh Framework Program (FP7/2007-2013) under grant agreement no. 254015. We thank Barbara Dutrow and an anonymous reviewer for their suggestions.

Editor: Helen Williams

Additional Information

Supplementary Information accompanies this letter at www.geochemicalperspectivesletters.org/article1719

Cite this letter as: van Hinsberg, V.J., Franz, G., Wood, B.J. (2017) Determining subduction-zone fluid composition using a tourmaline mineral probe. *Geochem. Persp. Let.* 3, 160–169.

References

Bebout, G., Ryan, J., Leeman, W. Bebout, A. (1999) Fractionation of trace elements by subduction-zone metamorphism—effect of convergent-margin thermal evolution. *Earth and Planetary Science Letters* 171, 63–81.

Connolly, J.A.D. (2005) Computation of phase equilibria by linear programming: A tool for geodynamic modeling and its application to subduction zone decarbonation. *Earth and Planetary Science Letters* 236, 524–541.

Elliott, T., Plank, T., Zindler, A., White, W. Bourdon, B. (1997) Element transport from slab to volcanic front at the Mariana arc. *Journal of Geophysical Research-Solid Earth* 102, 14991–15019.

Henry D.J., Dutrow, B.L. (1996) Metamorphic tourmaline and its petrologic applications. In: Grew E.S., Anovitz L.M. (Eds.) *Boron: Mineralogy, Petrology and Geochemistry. Reviews in Mineralogy* 33, 503–557.

Hermann, J. Rubatto, D. (2009) Accessory phase control on the trace element signature of sediment melts in subduction zones. *Chemical Geology* 265, 512–526.

Hermann, J., Spandler, C., Hack, A., Korsakov, A. (2006) Aqueous fluids and hydrous melts in high-pressure and ultra-high pressure rocks: Implications for element transfer in subduction zones. *Lithos* 92, 399–417.

Hoschek, G. (2007) Metamorphic peak conditions of eclogites in the Tauern Window, Eastern Alps, Austria: Thermobarometry of the assemblage garnet + omphacite + phengite + kyanite + quartz. *Lithos* 93, 1–16.

Keppler, H. (1996) Constraints from partitioning experiments on the composition of subduction-zone fluids. *Nature* 380, 237–240.

Kessel, R., Schmidt, M.W., Ulmer, P., Pettke, T. (2005) Trace element signature of subduction-zone fluids, melts and supercritical liquids at 120-180 km depth. *Nature* 437, 724–727.

Klimm, K., Blundy, J.D., Green, T.H. (2008) Trace element partitioning and accessory phase saturation during H_2O-saturated melting of basalt with implications for subduction zone chemical fluxes. *Journal of Petrology* 49, 523–553.

Leeman, W.P., Sisson, V.B. (1996) Geochemistry of boron and its implications for crustal and mantle processes. *Reviews in Mineralogy and Geochemistry* 33, 645–707.

Manning, C.E. (2004) The chemistry of subduction-zone fluids. *Earth and Planetary Science Letters* 223, 1–16.

Manning, C.E., Wilke, M., Schmidt, C., Cauzid, J. (2008) Rutile solubility in albite-H_2O and $Na_2Si_3O_7$-H_2O at high temperatures and pressures by in-situ synchrotron radiation micro-XRF. *Earth and Planetary Science Letters* 272, 730–737.

Marschall, H.R., Schumacher, J.C. (2012) Arc magmas sourced from mélange diapirs in subduction zones. *Nature Geoscience* 5, 862–867.

Rapp, J.F., Klemme, S., Butler, I.B., Harley, S.L. (2010) Extremely high solubility of rutile in chloride and fluoride-bearing metamorphic fluids: An experimental investigation. *Geology* 38, 323–326.

Scambelluri, M., Bottazzi, P., Trommsdorff, V., Vannucci, R., Hermann, J., Gomez-Pugnaire, M.T., Sanchez-Vizcaino, V.L. (2001) Incompatible element-rich fluids released by antigorite breakdown in deeply subducted mantle. *Earth and Planetary Science Letters* 192, 457–470.

Selverstone, J., Franz, G., Thomas, S., Getty, S. (1992) Fluid variability in 2 GPa eclogites as an indicator of fluid behavior during subduction. *Contributions to Mineralogy and Petrology* 112, 341–357.

Spandler, C., Hermann, J., Arculus, R., Mavrogenes, J. (2003) Redistribution of trace elements during prograde metamorphism from lawsonite blueschist to eclogite facies; implications for deep subduction-zone processes. *Contributions to Mineralogy and Petrology* 146, 205–222.

Spandler, C., Hermann, J., Arculus, R., Mavrogenes, J. (2004) Geochemical heterogeneity and element mobility in deeply subducted oceanic crust; insights from high-pressure mafic rocks from New Caledonia. *Chemical Geology* 206, 21–42.

Spandler, C., Mavrogenes, J., Hermann, J. (2007) Experimental constraints on element mobility from subducted sediments using high-P synthetic fluid/melt inclusions. *Chemical Geology* 239, 228–249.

Tatsumi, Y. (2005) The subduction factory: How it operates in the evolving Earth. *GSA today* 15, 4–10.

Tropper, P., Manning, C.E., Harlov, D.E. (2011) Solubility of $CePO_4$ monazite and YPO_4 xenotime in H_2O and H_2O-NaCl at 800°C and 1 GPa: Implications for REE and Y transport during high-grade metamorphism. *Chemical Geology* 282, 58–66.

Tsay, A., Zajacz, Z., Ulmer, P., Sanchez-Valle, C. (2017) Mobility of major and trace elements in the eclogite-fluid system and element fluxes upon slab dehydration. *Geochimica et Cosmochimica Acta* 198, 70–91.

van Hinsberg, V.J., Schumacher, J.C. (2007) Intersector element partitioning in tourmaline: a potentially powerful single crystal thermometer. *Contributions to Mineralogy and Petrology* 153, 289–301.

van Hinsberg, V.J., Schumacher, J.C., Kearns, S., Mason, P.R.D., Franz, G. (2006) Hourglass sector zoning in metamorphic tourmaline and resultant major and trace-element fractionation. *American Mineralogist* 91, 717–728.

van Hinsberg, V.J., Henry, D.J., Dutrow, B.L. (2011a) Tourmaline as a Petrologic Forensic Mineral: A Unique Recorder of Its Geologic Past. *Elements* 7, 327–332.

van Hinsberg, V.J., Henry, D.J., Marschall, H.R. (2011b) Tourmaline: an Ideal Indicator of Its Host Environment. *Canadian Mineralogist* 49, 1–16.

von Goerne, G., Franz, G. van Hinsberg, V.J. (2011) Experimental determination of Na–Ca distribution between tourmaline and fluid in the system CaO–Na_2O–MgO–Al_2O_3–SiO_2–B_2O_3–H_2O. *Canadian Mineralogist* 49, 137–152.

Zimmermann, R., Hammerschmidt, K., Franz, G. (1994) Eocene high pressure metamorphism in the Penninic units of the Tauern Window (Eastern Alps): evidence from ^{40}Ar-^{39}Ar dating and petrological investigations. *Contributions to Mineralogy and Petrology* 117, 175–186.

Determining subduction-zone fluid composition using a tourmaline mineral probe

V.J. van Hinsberg[1*], G. Franz[2], B.J. Wood[3]

Supplementary Information

The Supplementary Information includes:

- Analytical Methods
- Tauern Tourmaline
- *P–T* Constraints for Tourmaline Growth
- Constraints on the Nature and Composition of the Fluids
- Tourmaline–Fluid Partition Coefficients
- Data Sources for Figure 2
- Figures S-1 to S-3
- Tables S-1 to S-4
- Supplementary Information References

1. Department of Earth and Planetary Sciences, McGill University, Montreal, Quebec, Canada
* Corresponding author (email: V.J.vanHinsberg@gmx.net)
2. Department of Applied Geosciences, Technical University Berlin, Berlin, Germany
3. Department of Earth Sciences, University of Oxford, United Kingdom

Analytical Methods

Mineral major element compositions were determined by WDS-EMP, using the McGill University JEOL JXA-8900 microprobe (20kV, 15nA, focused beam). Natural minerals were used as primary standards with the tourmaline standards of Dyar *et al.* (2001) and an in-house tourmaline standard (UoB) as secondary references. Tourmaline analyses were converted to cations per formula unit using a Y + Z + T = 15 normalisation, or Si = 6 for analyses where the former resulted in Si in excess of 6. The precision, expressed as % RSD, is SiO_2 (1.1), TiO_2 (2.1) Al_2O_3 (1.1), MgO (2.9), MnO (11), FeO (2.0), CaO (4.8), Na_2O (2.0), K_2O (8), and F (15). Precision values for calculated cpfu are Si (0.7), Ti (1.6), Al (0.5), Mg (2.6), Mn (11), Fe (1.4), Ca (4.4), Na (1.8), K (8), and F (15). Accuracy, expressed as the average relative deviation in % for the secondary reference materials is SiO_2 (3), TiO_2 (-8) Al_2O_3 (4), MgO (-8), MnO (20), FeO (3), CaO (4), Na_2O (-1), K_2O (-22), and F (37), and for the calculated cpfu Si (0.3), Ti (-11), Al (0.5), Mg (-11), Mn (18), Fe (0.01), Ca (0.5), Na (-4.6), K (-26), and F (35). Trace element concentrations were determined by laser-ablation ICP-MS using a NewWave 213nm Nd:YAG laser at 10 Hz coupled to a Finnigan Element 2 magnetic sector mass spectrometer at the University of Bristol (La, Sm, Ba and Th; 15 and 30 µm spot size), and a PerkinElmer 6100 Elan DRC quadrupole ICP-MS at McGill University (60 µm spot size). Concentrations were standardised to NIST SRM 610 with Si from EMP as the internal reference element. Accuracy was estimated from measurements of the tourmaline standards of Dyar *et al.* (2001) and an in-house tourmaline standard (UoB), and is approximately 30 % relative, with significant exceptions V (6 %), Sr (-1 %), La (3 %), Nd (10 %), Hf (57 %) and U (95 %). EMP major element data are presented in Table S-1 and LA-ICP-MS trace element data in Tables S-2 and S-3. The major and trace element compositions of the tourmaline *a*-sectors have been used for all interpretations, because this sector is unaffected by sector zoning induced preferential elemental uptake or exclusion (see van Hinsberg *et al.*, 2006).

Table S-1 WDS electron-microprobe data for tourmaline growth zones, mineral inclusions in tourmaline, and matrix minerals. The values shown are the average for multiple analyses and their associated 1 standard deviation spread, except for omphacite where only one analysis was available. Normalisation factors used are the sum of cations for omphacite, titanite, plagioclase, amphibole and calcite, or the oxygen sum for phengite and biotite. Tourmaline was normalised to the sum of the elements residing at the Y, Z and T sites = 15, or Si = 6 cpfu, if the former resulted in Si > 6 cpfu.

	Tourmaline growth zones								Tourmaline growth zones								
	inner core	1s	mid core	1s	outer core 1	1s	outer core 2		1s	mantle	1s	inner rim	1s	mid rim	1s	outer rim	1s
SiO_2	37.9	0.4	38.1	0.4	38.3	0.2	38.2		0.7	38.7	0.5	36.0	0.2	35.9	0.3	36.2	0.3
TiO_2	0.44	0.05	0.39	0.03	0.42	0.10	0.25		0.03	0.19	0.02	0.18	0.05	0.36	0.09	0.35	0.08
Al_2O_3	29.1	0.3	29.3	0.2	29.7	0.7	30.8		0.1	31.8	0.3	28.2	0.3	28.7	0.2	28.4	0.4
MgO	10.3	0.4	10.0	0.2	10.2	0.2	10.1		0.1	12.8	0.1	10.7	0.4	9.5	0.3	9.5	0.3
MnO	0.004	0.008	0.01	0.01	0.004	0.006	0.01		0.02	0.007	0.009	0.008	0.007	0.002	0.004	0.007	0.008
FeO	9.67	0.84	10.30	0.43	9.06	1.01	8.08		0.05	3.04	0.10	2.73	0.31	3.79	0.48	4.43	0.82
CaO	1.2	0.1	0.93	0.06	1.1	0.1	0.64		0.05	1.6	0.2	1.3	0.3	0.56	0.08	0.9	0.2
Na_2O	2.48	0.05	2.59	0.01	2.54	0.10	2.83		0.02	2.32	0.10	2.1	0.2	2.49	0.09	2.1	0.2
K_2O	0.09	0.02	0.095	0.002	0.09	0.01	0.092		0.006	0.06	0.01	0.010	0.003	0.013	0.002	0.012	0.002
F	0.6	0.3	0.60	0.01	0.9	0.1	0.82		0.02	1.2	0.1	0.54	0.06	0.35	0.08	0.51	0.10
norm. factor	Y + Z + T = 15		Y + Z + T = 15		Y + Z + T = 15		Y + Z + T = 15			Y + Z + T = 15		Si = 6		Si = 6		Si = 6	
Si	5.92	0.02	5.93	0.02	5.95	0.03	5.94		0.08	5.93	0.04	6	-	6	-	6	-
Ti	0.052	0.006	0.046	0.003	0.049	0.012	0.029		0.004	0.022	0.002	0.022	0.006	0.05	0.01	0.04	0.01
Al	5.36	0.02	5.37	0.01	5.4	0.1	5.65		0.04	5.74	0.05	5.54	0.08	5.66	0.06	5.56	0.04
Mg	2.40	0.08	2.31	0.02	2.37	0.05	2.33		0.02	2.91	0.04	2.66	0.10	2.37	0.06	2.34	0.07
Mn	0.001	0.001	0.001	0.002	0.001	0.001	0.002		0.002	0.001	0.001	0.001	0.001	0.000	0.001	0.001	0.001
Fe	1.3	0.1	1.34	0.06	1.2	0.1	1.05		0.01	0.39	0.01	0.38	0.04	0.53	0.07	0.6	0.1
Ca	0.19	0.02	0.156	0.009	0.18	0.02	0.11		0.01	0.26	0.03	0.23	0.05	0.10	0.01	0.16	0.03
Na	0.75	0.02	0.781	0.007	0.76	0.03	0.85		0.01	0.69	0.03	0.68	0.05	0.81	0.04	0.68	0.06
K	0.018	0.003	0.0189	0.0002	0.018	0.003	0.018		0.001	0.012	0.003	0.002	0.001	0.0027	0.0005	0.0026	0.0004
F	0.3	0.1	0.295	0.002	0.42	0.07	0.41		0.01	0.57	0.06	0.28	0.03	0.18	0.04	0.27	0.06
X_{Mg}	0.66	0.03	0.63	0.01	0.67	0.03	0.69		0.00	0.88	0.00	0.87	0.02	0.82	0.02	0.79	0.04
dravite	0.50	0.01	0.51	0.01	0.52	0.04	0.60		0.01	0.62	0.03	0.60	0.04	0.5	0.3	0.5	0.2
schorl	0.27	0.03	0.29	0.01	0.26	0.01	0.27		0.00	0.08	0.00	0.09	0.02	0.12	0.07	0.13	0.05
uvite	0.19	0.02	0.16	0.01	0.18	0.02	0.11		0.01	0.26	0.03	0.23	0.05	0.08	0.04	0.14	0.06
foitite	0.037	0.004	0.044	0.002	0.042	0.015	0.023		0.018	0.040	0.014	0.09	0.01	0.3	0.4	0.3	0.3

Letter Geochemical Perspectives Letters

Table S-1 Cont.

	Mineral inclusions in tourmaline mantle									Matrix minerals							
	omphacite	1s	phengite	1s	titanite	1s				biotite	1s	plagioclase		amphibole		calcite	
SiO_2	53.9	-	48	1	29.6	0.4				37.1	1.7	59.1	0.2	51.5	0.8	0.03	0.02
TiO_2	0.04	-	0.20	0.07	34	3				0.5	0.4	< d.l.	-	0.09	0.03	0.01	0.02
Al_2O_3	5.9	-	24	1	4	2				14.6	0.9	21.5	0.2	6	1	0.001	0.001
MgO	11.3	-	4.6	0.5	0.04	0.02				19.7	0.7	0.01	0.01	17.7	0.8	0.47	0.09
MnO	0.03	-	0.004	0.006	0.009	0.008				0.02	0.01	< d.l.	-	0.02	0.01	0.09	0.10
FeO	5.3	-	2.0	0.3	0.7	0.3				9.7	0.8	0.14	0.06	8.3	0.5	0.33	0.09
CaO	17.9	-	< d.l.	-	28.3	0.3				< d.l.	-	3.47	0.09	10	2	55	1
Na_2O	4.2	-	0.2	0.2	0.02	0.01				0.16	0.07	9.5	0.1	2.0	0.8	< d.l.	-
K_2O	0.002	-	10.8	0.5	0.001	0.002				9	2	0.06	0.01	0.17	0.04	< d.l.	-
F	0.01	-	0.6	0.2	1.1	0.6				1.6	0.4	0.05	0.08	0.54	0.09	0.02	0.03
norm. factor	∑cat = 4		O = 11		∑cat = 3					O = 11		∑cat = 5		∑cat = 15		∑cat = 1	
Si	1.97	-	3.44	0.06	0.978	0.008				2.83	0.08	2.783	0.001	7.3	0.1	0.0005	0.0003
Ti	0.001	-	0.011	0.004	0.84	0.07				0.03	0.02	-	-	0.010	0.003	0.0002	0.0002
Al	0.25	-	1.99	0.09	0.15	0.06				1.3	0.1	1.191	0.007	0.9	0.2	0.0000	0.0000
Mg	0.62	-	0.49	0.06	0.0018	0.0009				2.24	0.09	0.001	0.001	3.7	0.2	0.012	0.002
Mn	0.001	-	0.0002	0.0004	0.0003	0.0002				0.001	0.001	-	-	0.003	0.001	0.001	0.001
Fe	0.16	-	0.12	0.02	0.019	0.008				0.62	0.05	0.005	0.002	0.99	0.05	0.005	0.001
Ca	0.70	-	-	-	1.004	0.003				-	-	0.175	0.004	1.5	0.2	0.982	0.002
Na	0.29	-	0.03	0.02	0.001	0.001				0.02	0.01	0.86	0.01	0.6	0.2	-	-
K	0.0001	-	0.98	0.04	0.0000	0.0001				0.9	0.2	0.004	0.001	0.03	0.01	-	-
F	0.001	-	0.14	0.05	0.12	0.06				0.4	0.1	0.01	0.01	0.24	0.04	0.001	0.002

Geochem. Persp. Let. (2017) 3, 160-169 | doi: 10.7185/geochemlet.1719 SI-6

Table S-2 Laser-ablation ICP-MS data for Ba, Th, La and Sm in tourmaline, and phengite and titanite inclusions. Most data represent the mean of multiple measurements. Uncertainties are the 1 standard deviation on the mean, or the count statistical error if only one measurement is available. Partition coefficients are those of Green and Adam (2003), combined with D $^{phg}/_{tur}$ from Klemme *et al.* (2011) and are used to calculate the Ba/Th and La/Sm ratios for the fluid. Analysis locations are shown in Figure 1.

Mineral	Concentrations in ppm							
	Ba	1 std	Th	1 std	La	1 std	Sm	1 std
Tur core - 1	1.1	0.3	0.009	0.006	0.008	0.007	0.09	0.07
Tur core - 1	3.0	0.7	0.03	0.02	0.04	0.02	0.08	0.10
Tur core - 2a	1.7	0.4	0.02	0.01	0.03	0.02	0.20	0.16
Tur core - 2b	1.9	1.0	0.02	0.02	0.012	0.006	0.08	0.09
Tur core - 2c	0.9	0.2	0.007	0.008	0.03	0.01	0.13	0.06
Tur mantle - 3	2	2	0.011	0.005	0.005	0.006	0.028	0.008
Tur rim - 4	0.81	0.07	0.009	0.001	0.004	0.003	0.04	0.01
Tur rim - 5	0.8	0.9	0.02	0.02	0.036	0.003	0.031	0.005
Phengite	1908	183	0.012	0.005	0.02	0.01	0.04	0.04
Titanite	55	73	0.6	0.7	0.45	0.04	5	3

Mineral	Partition coefficients (min/fl)				Ratios	
	Ba	Th	La	Sm	Ba/Th fluid	La/Sm fluid
Tur core - 1	0.06	0.88	1.08	1.50	1795	0.12
Tur core - 1	0.06	0.88	1.08	1.50	1770	0.64
Tur core - 2a	0.06	0.88	1.08	1.50	1397	0.18
Tur core - 2b	0.06	0.88	1.08	1.50	1950	0.22
Tur core - 2c	0.06	0.88	1.08	1.50	2088	0.30
Tur mantle - 3	0.06	0.88	1.08	1.50	2813	0.27
Tur rim - 4	0.06	0.88	1.08	1.50	1443	0.17
Tur rim - 5	0.06	0.88	1.08	1.50	729	1.64
Phengite	91.2	1.53	3.84	6.07	2782	0.92
Titanite	0.15	4.4	18.5030	173.8290	2710	0.79

Table S-3 Laser-ablation ICP-MS trace element data for tourmaline, and phengite and titanite inclusions. The tourmaline data represent the mean of multiple measurements and the uncertainties reported are 1 standard deviation on this mean. For phengite and titanite, we report the count statistical error. Measurements were corrected for differences in ablation behaviour between standards and samples by normalising to EMP Si-content.

Conc in ppm	Tourmaline				Inclusions			
Element	Rim of core	1 std	Mantle	1 std	Phengite	1 std cse	Titanite	1 std cse
Li	31	3	74	10	250	6	19	2
V	65	4	64.1	0.8	71.6	0.9	94	3
Cr	209	20	139	44	122	2	299	9
Mn	26.6	0.6	17	1	11.6	0.4	17.1	0.8
Cs	0.07	0.04	0.07	0.02	26.1	0.3	0.07	0.03
Sr	1107	28	1376	132	42.4	0.8	387	13
Ba	0.9	0.6	0.6	0.2	1778	17	3.8	0.6
Ti	805	116	1312	461	941	90	188700	15341
Nb	< d.l.		0.02		1.04	0.07	77	2
Ta	0.007	0.006	0.02		0.12	0.02	3.5	0.2
Zr	< d.l.		3	6	0.07	0.03	16	4
Hf	< d.l.		0.1	0.1	0.003	0.005	0.5	0.1
La	< d.l.		0.001	0.001	0.01	0.01	0.48	0.05
Ce	< d.l.		0.014	0.002	0.010	0.006	3.4	0.2
Sm	< d.l.		0.024	0.006	0.04	0.04	3.4	0.4
Lu	< d.l.		0.007	0.002	< d.l.		0.56	0.07
Y	0.03	0.02	0.02	0.03	0.06	0.02	36	2
Pb	13	4	6.7	0.3	2.4	0.7	14	4
Th	0.01	0.01	0.01	0.01	0.015	0.009	0.09	0.03
U	0.002	0.001	0.008	0.006	0.000	0.004	1.3	0.1

< d.l. Value below detection limit

Tauern Tourmaline

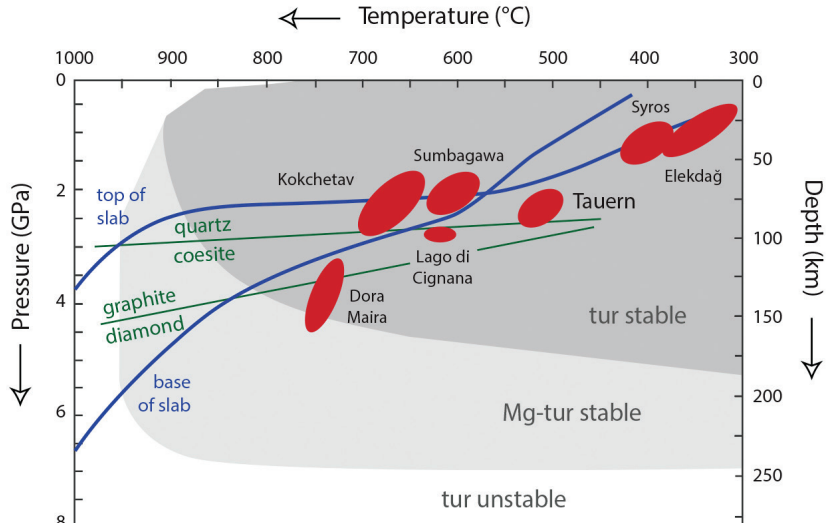

Figure S-1 Tourmaline is stable for most of the *P–T* range typically found in subduction zones, and is an accessory phase in exposed subduction-zone lithologies for all the terrains shown. Typical subduction path (blue solid lines) from Syracuse *et al.* (2010) and *P–T* estimates for subduction-zone terrains from Zimmermann *et al.* (1994) and Marschall *et al.* (2009). Tourmaline stability fields from van Hinsberg *et al.* (2011b).

The grain investigated here (inventory number 2013/13, Mineralogical Museum, Technical University Berlin) is a ~2 mm long black tourmaline. It has an irregular brown core that likely grew as an interstitial phase, mantled by an idiomorphic, compositionally homogenous rim, and a strongly zoned outer rim that fingers into the enclosing minerals (Fig. S-2a). The inner core and mantle are homogenous in composition, whereas the outer core and rim are strongly compositionally zoned (Fig. 1), suggesting that the former represent punctuated growth events, whereas the latter record growth by gradual boron release. Only quartz and rutile inclusions are found in the core, whereas the mantle contains inclusions of the peak metamorphic minerals (see Zimmermann *et al.*, 1994; Hoschek, 2007), omphacite (partially replaced by amphibole), titanite and phengite, as well as negative crystal forms of garnet (Fig. S-2d). The outermost rim is in equilibrium with the matrix minerals. These inclusion parageneses suggest formation of the core prior to peak metamorphism, *i.e.* prograde; formation of the mantle at, or after peak metamorphism; and late-stage growth of the rim following re-appearance of amphibole. Back-scattered electron images reveal fine compositional heterogeneity in the core (Fig. S-2c), interpreted as outlining an original mica foliation and suggests that tourmaline overgrew mica during growth.

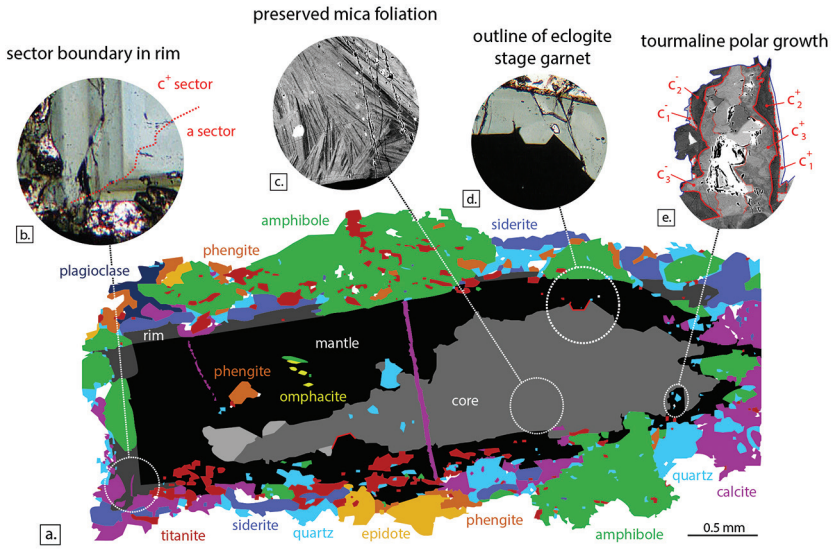

Figure S-2 Petrography of the Tauern tourmaline grain used in this study. **(a)** Mineral-map showing its inclusion and matrix mineralogy, and the core, mantle and rim zones of the tourmaline grain. This map is based on back-scattered electron imaging and WDS-EMP element mapping for Ca, Mg, Ti, Fe, Si and Na. **(b)** Example of hourglass sector zoning in the outermost rim in PPL microscopy. **(c)** Back-scattered electron image of compositional heterogeneity in the tourmaline core, outlining the foliation of protolith mica grains overgrown by tourmaline. **(d)** Outline of an idiomorphic eclogite-stage garnet grain replaced during growth of the mantle zone in PPL microscopy. **(e)** Back-scattered electron image of c^+-c^- polar tourmaline growth.

The tourmaline grain has a dravite-dominated composition (Henry *et al.*, 2011), with variable proportions of the uvite (0.05 to 0.3), schorl (0.05 to 0.3) and foitite (0.01 to 0.3) end-members (Table S-1). Al-contents are consistently below 6, indicating significant Mg and/or Fe at the Z-site. The X-site vacancy content is low, but shows a marked increase in the rim, in agreement with the negative correlation between metamorphic grade and X-site vacancy content (Henry and Dutrow, 1996).

P–T Constraints for Tourmaline Growth

The tourmaline grain displays compositional hourglass-style sector zoning in core, mantle and rim, as well as polar growth (Fig. S-2b,e), and this allows temperatures of formation to be determined from inter-sector thermometry (Henry and Dutrow, 1996; van Hinsberg and Schumacher, 2007b). Temperatures calculated using the Ca and Ti thermometric formulations of van Hinsberg and Schumacher (2007b) are consistent, and results for inter-polar and inter-sector pairs agree within uncertainty (Fig. 1f). Mantle zone temperatures show significant scatter,

which is attributed to rapid growth of this zone leading to diffusion unable to keep up with growth. Equilibrium separation of Ca and Ti was, therefore, not achieved. As such, inter-sector partition coefficients, and hence temperatures will be underestimates for the mantle growth zone.

Tourmaline barometry has yet to be established, but its K-content has been suggested as a pressure-indicator based on characteristically high K-contents in UHP tourmalines (*e.g.,* Shimizu and Ogasawara, 2013), thermodynamic considerations (van Hinsberg and Schumacher, 2007a) and experimental studies (Berryman *et al.*, 2014, 2015). However, this correlation between K-content and *P* is not always consistent (*e.g.,* Marschall *et al.*, 2009), as it also depends on the exchanging mineral phases and bulk K-content (Berryman *et al.*, 2015). For the Tauern tourmaline, the dominant K-exchanging phase is phengite, and its presence as inclusions (Fig. S-2a) and as a matrix phase, as well as its ubiquitous occurrence in the Tauern Eclogite Zone at various metamorphic grades (Zimmermann *et al.*, 1994; Hoschek, 2007) suggests that phengite was present throughout tourmaline's growth history. The K-content in the *a*-sector of the tourmaline grain is therefore interpreted as predominantly controlled by *P*, and used as a qualitative barometer (Fig. 1g).

Constraints on the Nature and Composition of the Fluids

Sector zoning in tourmaline develops in equilibrium on the growth surfaces, but is subsequently in disequilibrium in the crystal bulk (van Hinsberg *et al.*, 2006; see also Hollister, 1970). Re-equilibration is governed by volume diffusion rates, and the preservation of sector zoning in this Tauern tourmaline grain proves that primary compositions are preserved. The compositions of the subsequent growth zones can, therefore, be used to track the evolving composition of its host environment throughout subduction and uplift. Based on tourmaline compositions, textures, and *P–T* history, we interpret the core to have formed from internal release of B, thus recording the compositions of fluids released from the progressively subducting slab (Fig. 1a); the mantle zone to represent growth by metasomatic input of B after detachment of the Tauern Eclogite Zone from the slab and its transfer to the overriding plate, and hence recording fluids flushing the subduction channel that were released in deeper slab devolatilisation (*i.e.* those recorded by the outermost core); and the rim to track the uplift after merging with the hanging and footwall tectonic units. In this interpretation, the core represents growth from internal release of B in prograde metamorphic reactions, and hence records locally derived fluids in equilibrium with the evolving blueschist to eclogite mineral paragenesis. Fluid heterogeneity on a local scale is possible at this stage (*cf.* Selverstone *et al.*, 1992), but this will decrease as the temperature, and hence element diffusivities, increase. The inner core growth zones are large and subsequent core zones progressively narrower, which is in agreement with most B being released early in prograde metamorphism (*e.g.,* Bebout *et al.*, 1999; van Hinsberg *et al.*, 2011a). The eclogite-facies minerals can be expected to contain little B, except for that sequestered in tourmaline (*e.g.,*

Bebout *et al.*, 1993, 1999; Marschall *et al.*, 2006), and the mantle growth zone is, therefore, interpreted to have formed from externally derived, metasomatising fluids. Addition of B can also explain the replacement of garnet by tourmaline (Fig. S-2d) despite it being a stable phase at these *P–T* conditions (see Zimmermann *et al.*, 1994; Hoschek, 2007), because tourmaline is predicted to replace the aluminous phases preferentially as B is progressively added (van Hinsberg and Schumacher, 2007a). The lack of compositional zoning in the mantle growth zone suggests growth in a single event, followed by continuous rim growth. The lack of a clear compositional break between mantle and inner rim suggests a common fluid source, although this fluid changes in composition as the rocks are exhumed. The outer rim has a distinctly different composition, especially in X_{Ca}, and *T* and X_{Mg} display a kink (Fig. 1).

For these specific tourmaline compositions there is no crystal-chemical limitation to F incorporation (Henry and Dutrow, 2011), and F-contents likely track that of the fluid. High F-contents in the mantle zone match elevated F in associated titanite, which has been attributed to a high fluid F-activity (Franz and Spear, 1985). Whereas the outermost core has a similar F-content to that of the mantle zone and is, therefore, consistent with a fluid link between these growth zones as proposed above, this is not true for X_{Ca} (Fig. 1e). This indicates modification of slab-released fluids in the subduction channel prior to being recorded by tourmaline in the overriding plate, and is in agreement with predicted Ca and Na behaviour (*e.g,* Manning, 2004). Na concentrations in the fluid can be estimated from experimental tourmaline–fluid partitioning relationships (von Goerne *et al.*, 2001; Berryman *et al.*, 2015) combined with tourmaline *a*-sector Na concentrations. Calculated Na contents vary from 0.45 to 0.75 mol L^{-1} with *P–T*, and are highest for the outermost core. Sodium is likely a dominant solute in subduction-zone fluids (*e.g.,* Manning, 2004), and these reconstructed Na contents indicate that the fluids released from the subducting slab are relatively dilute, in good agreement with theoretical considerations and experimental results (Selverstone *et al.*, 1992; Manning, 2004; Kessel *et al.*, 2005; Hermann *et al.*, 2006; Spandler *et al.*, 2007; Tsay *et al.*, 2017).

Tourmaline is stable in acidic aqueous solutions and dissolves at high pH (*e.g.,* Henry and Dutrow, 1996). A constraint on pH for the tourmaline mantle zone can be obtained from the reaction:

$$3\ NaAlSi_2O_6 + 2\ H^+_{(aq)} = NaAl_3Si_3O_{10}(OH)_2 + 2\ Na^+_{(aq)} + 3\ SiO_2$$

$$3\ \text{jadeite} + 2\ H^+_{(aq)} = \text{paragonite} + 2\ Na^+_{(aq)} + 3\ \text{quartz}$$

the Na concentration reconstructed above, and the jadeite and paragonite activities in omphacite and phengite mineral inclusions, respectively. Thermodynamic properties for minerals and aqueous species were calculated using the Holland and Powell (2011) database and its associated activity models (this database uses a modified version of the density model of Anderson *et al.* (1991) to calculate properties for aqueous species at elevated *P* and *T*). This results in a pH estimate of 0.8, which is 1.7 pH units below the neutral point of water at these conditions.

The F content of this solution can similarly be estimated from the reaction:

$$CaTiSiO_5 + NaAlSi_2O_6 + HF_{(aq)} = CaAlSiO_4F + TiO_2 + 2\ SiO_2 + Na^+_{(aq)} + OH^-_{(aq)}$$

$$\text{titanite} + \text{jadeite} + HF_{(aq)} = \text{“F-titanite”} + \text{rutile} + 2\,\text{quartz} + Na^+_{(aq)} + OH^-_{(aq)}$$

Thermodynamic data were sourced as above, except for thermodynamic properties and activity models for titanite, which were taken from Tropper *et al.* (2002), and the ΔG_f (T,P) for $HF_{(aq)}$, which was estimated from the fluorite solubility data of Tropper and Manning (2007). Estimated F-concentrations are 1.8 ppmm for the average composition of titanite inclusions, and 3.1 ppmm for the most F-rich titanite zones in these inclusions. This concentration is surprisingly low, which could indicate that species other than HF are the dominant F-species at these conditions (see also Tropper and Manning, 2007). An upper constraint on F-content is given by the saturation concentration of fluorite, which is approximately 1400 ppmm at these conditions (Tropper and Manning, 2007), when assuming m $Cl_{(aq)}$ = m $Na_{(aq)}$. Fluorite has been found in marbles of the Tauern Eclogite Zone (Franz and Spear, 1985), but not in this sample.

Tourmaline–Fluid Partition Coefficients

Mineral–fluid trace element partition coefficients allow fluid composition to be calculated from the compositions of the minerals that grew from this fluid, assuming equilibrium between minerals and fluid. At present, these D-values are not known for tourmaline, nor for titanite. These were estimated here by combining partitioning data for natural tourmaline–phengite and titanite–phengite mineral pairs in subduction-zone rocks from Syros, Greece (Marschall, 2005; Klemme *et al.*, 2011) with experimentally determined high-*P* phengite-fluid D-values (Green and Adam, 2003) in an approach similar to that used by Keppler (1996). The D-values used are given in Table S-4.

There are two main uncertainties in this approach. First, fluid concentrations reported by Green and Adam (2003) are based on an assumed total dissolved solid (TDS) content of 50 wt. %. This is higher than most experimental values (*e.g.,* Kessel *et al.,* 2005; Tsay *et al.,* 2017), although high TDS values have been reported for fluid inclusions in eclogite minerals (*e.g.,* Scambelluri and Phillipot, 2001). The 50 wt. % TDS assumption of Green and Adam (2003) only impacts the absolute concentrations calculated from the estimated $D^{tur}/_{fl}$. Element ratios are unaffected. For example, if a TDS of 25 wt. % would be assumed instead, all fluid concentrations in Figure 2 would half, but the ratios plotted in Figure 3 would be identical.

Secondly, the Syros $D^{phg}/_{tur}$ values used to derive $D^{tur}/_{fl}$ are for ~1 GPa at 450 ˚C, whereas tourmaline growth took place from peak conditions of 2.1 GPa at 500 ˚C to rim retrograde conditions of 0.3 GPa and 350 ˚C (Fig. 1a). Moreover, the $D^{phg}/_{fl}$ data of Green and Adam (2003) are for experimental conditions of 3 GPa and 600–700 ˚C. This mismatch in *P–T* conditions can impact calculated fluid compositions, because D-values have a *P–T* dependence, both in their absolute values and in the relative D-values among the elements (*e.g.,* Blundy and Wood, 2003). This therefore introduces uncertainty in both the absolute concentrations of the fluid calculated from tourmaline compositions and elemental patterns.

Table S-4 Partition coefficients used in this study. Tourmaline-fluid and titanite-fluid coefficients were calculated by combining the phengite-tourmaline and phengite-titanite intermineral partition coefficients for Syros sample SY309B (Klemme *et al.*, 2011; Marschall, 2005) with phengite-fluid experimental partition coefficients from Green and Adam (2003).

Element	Phg/Tur	Phg/fluid	Tur/fluid	Ttn/fluid
Li	5.3	2.0	0.4	0.004
B	0.004	0.94	233	0.001
V	1.25	223	179	327
Cr	3.0	287	95	
Mn	2.8	11	4.0	29
Rb	250	108	0.4	0.9
Cs	25	7.8	0.3	0.8
Sr	0.20	1.4	6.9	13
Ba	1635	91	0.06	0.15
Ti	0.40	75	187	
Nb	24	7.1	0.3	1929
Ta	34	51	1.5	471
Zr	2.2	2.9	1.4	21
Hf	4.0			
La	3.6	3.8	1.1	19
Ce	3.1	3.3	1.1	155
Nd	3.3			
Sm	4.0	6.1	1.5	174
Eu	5.4			
Gd	1.6			
Dy	1.7			
Er	2.8			
Yb	9.3			
Lu	4.0	11	2.8	1618
Y	4.0	24	6.0	
Pb	4.2	43	10	116
Th	1.7	1.5	0.9	0.9
U	0.93	1.6	1.7	4.5

To evaluate the impact on calculated fluid compositions from changes in D-values with *P–T*, the D-values were modelled using Lattice-Strain Theory (LST; see Onuma *et al.*, 1968; Brice, 1975; Blundy and Wood, 1994, 2003; Wood and Blundy, 2003). This allows for extrapolating a LST fit of $D^{phg}/_{fl}$ to the *P–T* conditions of interest using the *P–T* dependence of phengite lattice dimensions and elasticity and phengite solubility to account for changes in the partitioning behaviour of the mineral, and changes in the aqueous element speciation to

model the fluid. Lattice dimensions, and changes therein with *P–T*, control a mineral's trace element size preferences, lattice elasticity determines the contrast in partition coefficients among the elements, and mineral solubility their absolute values, whereas aqueous speciation impacts the availability of elements for incorporation into the mineral (see Blundy and Wood, 1994; Wood and Blundy, 2003; van Hinsberg *et al.*, 2010, and references therein).

The experimental $D^{phg}/_{fl}$ values of Green and Adam (2003) were fit to LST equations to obtain r_0, D_0 and E parameters (the ideal site radius, D at this ideal radius, and site elasticity, respectively; Blundy and Wood, 1994). The r_0 and E parameters were subsequently extrapolated to relevant *P–T* conditions using independently-determined *P–T* dependence of white mica lattice constants (r_0: Guggenheim *et al.*, 1987; Gatta *et al.*, 2010, E: McNeil and Grimsditch, 1993; Curetti *et al.*, 2006). The D_0 parameter tracks changes in mineral solubility, but, unfortunately, literature data on white mica solubility and its dependence on *P–T* are inconsistent (*cf.* Melzer and Wunder, 2000; Green and Adam, 2003). Qualitatively, mineral solubility is expected to increase with temperature, but decrease with pressure, and the net effect on D_0 may thus be small for the 200 °C and 2.4 GPa extrapolation required from experimental to Syros conditions. D_0 was therefore assumed to be constant. Phengite-fluid partition coefficients can then be extrapolated to the *P–T* conditions of interest.

Two approaches were explored to calculate the $D^{tur}/_{fl}$ at conditions of Tauern tourmaline growth. In the first, the same approach as that used for $D^{phg}/_{fl}$ extrapolation was used. $D^{phg}/_{fl}$ extrapolated to 1 GPa and 450 °C was combined with minimum Syros $D^{phg}/_{tur}$ to estimate $D^{tur}/_{fl}$ at these conditions. These tourmaline-fluid D-values were subsequently fit to the LST equation, and r_0 and E parameters were then extrapolated to Tauern conditions using tourmaline lattice systematics reported by Xu *et al.* (2016). Scarcity of D-values (*e.g.*, only three data points for the 3+ elements), as well as uncertainties in element site occupancy in the tourmaline structure, complicates the LST fits. Moreover, changes in D_0 cannot be modelled for lack of data on tourmaline solubility. As an alternative, $D^{tur}/_{fl}$ was calculated by extrapolating $D^{phg}/_{fl}$ to Tauern conditions and assuming constant $D^{phg}/_{tur}$. Phengite-tourmaline D-values do appear to increase with pressure (Klemme *et al.*, 2011), and this approach will thus lead to underestimated trace element concentrations in the fluid at high pressure. However, the LST fit of $D^{phg}/_{fl}$ is better constrained than that of $D^{tur}/_{fl}$, as is the *P–T* dependence of phengite lattice dimensions and elasticity. The second approach is therefore preferred.

Aqueous element speciation and changes therein with P and T also impact partition coefficients by changing the availability of the species dominantly involved in element uptake (van Hinsberg *et al.*, 2010). Whereas free ions become more abundant with increasing P, increasing T favours associated species (*e.g.*, Manning, 2004). Metal-silicate species are likely important at subduction zone conditions (Manning *et al.*, 2008; Wilke *et al.*, 2012; Tsay *et al.*, 2017) and may represent the dominant element uptake vector into silicate minerals, but lack of data on their stability constants precludes modelling of these species. Instead,

the relative abundance of metal-(hydr)oxide species at varying *P–T* was modelled for a Tauern fluid composition at a tourmaline-reconstructed salinity of 0.6 mol L^{-1} NaCl using the *hkf*-model and the latest version of the SUPCRT database (Johnson *et al.*, 1992). This makes the implicit assumption that (hydr)oxide species are a more important element uptake vector in phengite and tourmaline than free ions and Cl-species.

Figure S-3 shows the results of this modelling by comparing $^{Ba}/_{Th}$ *vs.* $^{La}/_{Sm}$ ratios in the reconstructed Tauern fluids as calculated assuming, in Figure S-3a, constant $D^{tur}/_{fl}$, and, in Figure S-3b, variable $D^{tur}/_{fl}$ calculated from extrapolated $D^{phg}/_{fl}$, assuming constant $D^{phg}/_{tur}$. The overall trend is identical, but $^{Ba}/_{Th}$ and $^{La}/_{Sm}$ both shift to lower values. Fluids reconstructed from phengite inclusions in the tourmaline mantle remain consistent when using the extrapolated $D^{phg}/_{fl}$ (titanite D-values were not extrapolated and the titanite-reconstructed fluid is therefore not plotted). Changes in speciation are predicted to lower $^{Ba}/_{Th}$ for the prograde tourmaline zones, and increase it for the retrograde rim, with the mantle zone unaffected. These shifts are entirely owing to changes in Ba-speciation, as changes in Th-speciation are expected to be negligible (Bailey and Ragnarsdottir, 1994). The impact on $^{La}/_{Sm}$ is estimated to lower the ratio for all growth zones, but the shift is small given the similarity in speciation among the REE.

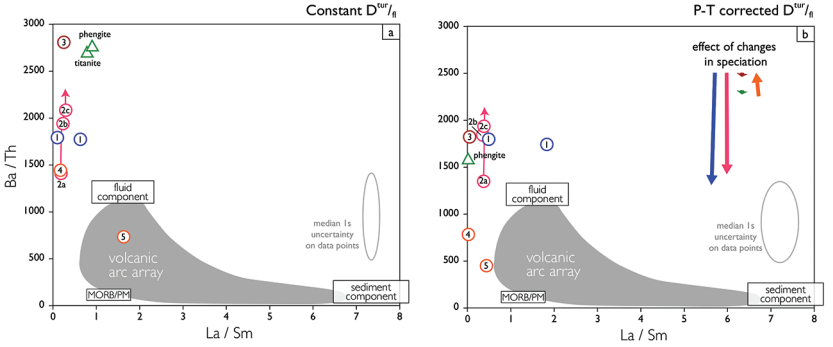

Figure S-3 Reconstructed $^{Ba}/_{Th}$ *vs.* $^{La}/_{Sm}$ ratios for subduction-zone fluids in the Tauern eclogite zone, as determined from tourmaline compositions (see Fig. 2 for locations of these points). **(a)** Calculated assuming constant $D^{tur}/_{fl}$, obtained by combining experimentally determined $D^{phg}/_{fl}$ of Green and Adam (2003) with $D^{phg}/_{tur}$ of Klemme *et al.* (2011). **(b)** Calculated from $D^{phg}/_{fl}$ of Green and Adam (2003) extrapolated to relevant *P–T* conditions using phengite lattice systematics at constant $D^{phg}/_{tur}$ (from Klemme *et al.*, 2011). The impact of changing speciation on $D^{tur}/_{fl}$ is shown by the thick arrows. Reconstructing fluid compositions with extrapolated D values results in lower $^{Ba}/_{Th}$ in the fluid, with only minimal impact on $^{La}/_{Sm}$. The differences in $^{Ba}/_{Th}$ between core and mantle become smaller, but the predicted effect of changes in speciation would re-introduce this difference. The gray uncertainty ellipses show the 1 standard deviation uncertainty in the ratios resulting from the spread in the trace element analyses of the minerals.

In conclusion, the impact of using estimated tourmaline-fluid element partition coefficients on results presented in Figure 3 is small and does not change its interpretation. There is too much uncertainty in the D-value LST extrapolations to make a quantitative assessment of the impact on the absolute concentrations shown in Figure 2. However, there is good agreement among the fluid concentrations reconstructed from tourmaline and from co-genetic phengite and titanite, suggesting that the precision in reconstructed fluid compositions is approximately an order of magnitude. The reconstructed concentrations of Ti are consistent with a rutile-saturated fluid as determined from rutile solubility experiments (Manning *et al.*, 2008; Rapp *et al.*, 2010; Hayden and Manning, 2011; Tsay *et al.*, 2017), and LILE and REE concentrations similarly agree within an order of magnitude with eclogite-fluid experiments buffered by non-end-member allanite (Tsay *et al.*, 2017) for the estimated F-contents in Tauern solutions derived above, as shown in Figure 2. The best estimate of the uncertainty in the absolute concentrations presented in Figure 2 is thus that these are precise and accurate to within an order of magnitude.

Data Sources for Figure 2

Fluid concentrations reconstructed from eclogite-facies minerals for other palaeo-subduction zones shown in Figure 2a were calculated from the average garnet, omphacite and phengite compositions reported for samples DM9 and DM30 from Dora Maira (Hermann, 2002), samples SY309, 412, 413 and 420 from Syros (Marschall, 2005) and samples 803, 1008 and 1101 from New Caledonia (Spandler *et al.*, 2003). These mineral data were combined with the experimental mineral-fluid trace element partition coefficients of Green and Adam (2003) to reconstruct the compositions of the fluids from which these minerals formed. Experimental data shown are from Tsay *et al.* (2017) and represent the composition of a fluid in equilibrium with eclogite at 590 °C and 2.4 GPa in H_2O, and at 680 °C and 2.5 GPa in a fluid with 1 mol L^{-1} NaF. Symbols with arrows indicate maximum values as defined by the relevant detection limit. Figure 2b shows MORB-normalised compositions of average volcanic arc rocks (calculated from the Georoc database – http://georoc.mpch-mainz.gwdg.de/), fluid inclusions in eclogite-facies olivine (samples AL9854B and AL9854, Scambelluri *et al.*, 2001), the H_2O-experiment of Tsay *et al.* (2017), and the median and associated interquartile range of the reconstructed fluids shown in Figure 2a for the Tauern, Dora Maira, Syros and New Caledonia palaeo-subduction zones.

Supplementary Information References

Anderson, G.M., Castet, S., Schott, J., Mesmer, R.E. (1991) The density model for estimation of thermodynamic parameters of reactions at high temperatures and pressures. *Geochimica et Cosmochimica Acta* 55, 1769–1779.

Bailey, E.H., Ragnarsdottir, K.V. (1994) Uranium and thorium solubilities in subduction zone fluids. *Earth and Planetary Science Letters* 124, 119–129.

Bebout, G.E., Ryan, J.G., Leeman, W.P. (1993) B–Be systematics in subduction-related metamorphic rocks: characterization of the subducted component. *Geochimica et Cosmochimica Acta* 57, 2227–2237.

Berryman, E., Wunder, B., Rhede, D. (2014) Synthesis of K-dominant tourmaline. *American Mineralogist* 99, 539–542.

Berryman, E., Wunder, B., Wirth, R., Rhede, D., Schettler, G., Franz, G., Heinrich, W. (2015) An experimental study on K and Na incorporation in dravitic tourmaline and insight into the origin of diamondiferous tourmaline from the Kokchetav Massif, Kazakhstan. *Contributions to Mineralogy and Petrology* 169, 1–16.

Blundy, J., Wood, B. (1994) Prediction of crystal-melt partition-coefficients from elastic-moduli. *Nature* 372, 452–454.

Blundy, J., Wood, B. (2003) Partitioning of trace elements between crystals and melts. *Earth and Planetary Science Letters* 210, 383–397.

Brice, J. (1975) Some thermodynamic aspects of the growth of strained crystals. *Journal of Crystal Growth* 28, 249–253.

Curetti, N., Levy, D., Pavese, A., Ivaldi, G. (2006) Elastic properties and stability of coexisting 3T and 2M(1) phengite polytypes. *Physics and Chemistry of Minerals* 32, 670–678.

Dyar, M., Wiedenbeck, M., Robertson, D., Cross, L., Delaney, J., Ferguson, K., Francis, C., Grew, E., Guidotti, C., Hervig, R., Hughes, J., Husler, J., Leeman, W., McGuire, A., Rhede, D., Rothe, H., Paul, R., Richards, I., Yates, M. (2001) Reference minerals for the Microanalysis of light elements. *Geostandards Newsletter-The Journal of Geostandards and Geoanalysis* 25, 441–463.

Franz, G., Spear, F. (1985) Aluminous titanite(sphene) from the eclogite zone, south-central Tauern Window, Austria. *Chemical Geology* 50, 33–46.

Gatta, G.D., Rotiroti, N., Lotti, P., Pavese, A., Curetti, N. (2010) Structural evolution of a 2M (1) phengite mica up to 11 GPa: an in situ single-crystal X-ray diffraction study. *Physics and Chemistry of Minerals* 37, 581–591.

Green, T.H., Adam, J. (2003) Experimentally-determined trace element characteristics of aqueous fluid from partially dehydrated mafic oceanic crust at 3.0 GPa, 650-700 °C. *European Journal of Mineralogy* 15, 815–830.

Guggenheim, S., Chang, Y.-H., Koster van Groos, A.F. (1987) Muscovite Dehydroxylation - High-Temperature Studies. *American Mineralogist* 72, 537–550.

Hayden, L.A., Manning, C.E. (2011) Rutile solubility in supercritical $NaAlSi_3O_8$-H_2O fluids. *Chemical Geology* 284, 74–81.

Henry D.J. Dutrow B.L. (1996) Metamorphic tourmaline and its petrologic applications. In: Grew E.S., Anovitz L.M. (Eds.) *Boron: Mineralogy, Petrology and Geochemistry. Reviews in Mineralogy* 33, 503-557.

Henry, D.J., Dutrow, B.L. (2011) The Incorporation of Fluorine in Tourmaline: Internal Crystallographic Controls or External Environmental Influences? *Canadian Mineralogist* 49, 41–56.

Henry, D.J., Novak, M., Hawthorne, F.C., Ertl, A., Dutrow, B.L., Uher, P., Pezzotta, F. (2011) Nomenclature of the tourmaline-supergroup minerals. *American Mineralogist* 96, 895–913.

Hermann, J. (2002) Allanite: thorium and light rare earth element carrier in subducted crust. *Chemical Geology* 192, 289–306.

Hermann, J., Spandler, C., Hack, A., Korsakov, A. (2006) Aqueous fluids and hydrous melts in high-pressure and ultra-high pressure rocks: Implications for element transfer in subduction zones. *Lithos* 92, 399–417.

Holland, T.J.B., Powell, R. (2011) An improved and extended internally consistent thermodynamic dataset for phases of petrological interest, involving a new equation of state for solids. *Journal of Metamorphic Geology* 29, 333–383.

Hollister, L. (1970) Origin, mechanism, and consequences of compositional sector-zoning in staurolite. *American Mineralogist* 55, 742–766.

Hoschek, G. (2007) Metamorphic peak conditions of eclogites in the Tauern Window, Eastern Alps, Austria: Thermobarometry of the assemblage garnet + omphacite + phengite + kyanite + quartz. *Lithos* 93, 1–16.

Johnson, J.W., Oelkers, E.H., Helgeson, H.C. (1992) SUPCRT92 - A software package for calculating the standard molal thermodynamic properties of minerals, gases, aqueous species, and reactions from 1 to 5000 bar and 0 to 1000°C. *Computers and Geosciences* 18, 899–947.

Keppler, H. (1996) Constraints from partitioning experiments on the composition of subduction-zone fluids. *Nature* 380, 237–240.

Klemme, S., Marschall, H.R., Jacob, D.E., Prowatke, S., Ludwig, T. (2011) Trace-Element Partitioning and Boron Isotope Fractionation Between White Mica and Tourmaline. *Canadian Mineralogist* 49, 165–176.

Klimm, K., Blundy, J.D., Green, T.H. (2008) Trace element partitioning and accessory phase saturation during H_2O-saturated melting of basalt with implications for subduction zone chemical fluxes. *Journal of Petrology* 49, 523–553.

Manning, C.E. (2004) The chemistry of subduction-zone fluids. *Earth and Planetary Science Letters* 223, 1–16.

Manning, C.E., Wilke, M., Schmidt, C., Cauzid, J. (2008) Rutile solubility in albite-H_2O and $Na_2Si_3O_7$-H_2O at high temperatures and pressures by in-situ synchrotron radiation micro-XRF. *Earth and Planetary Science Letters* 272, 730–737.

Marschall, H.R. (2005) Lithium, Beryllium and Boron in High-Pressure Metamorphic Rocks from Syros (Greece). PhD thesis, Universität Heidelberg. http://www.ub.uni-heidelberg.de/archiv/5634.

Marschall, H.R., Altherr, R., Ludwig, T., Kalt, A., Gméling, K., Kasztovszky, Z.S. (2006) Partitioning and budget of Li, Be and B in high-pressure metamorphic rocks. *Geochimica et Cosmochimica Acta* 70, 4750–4769.

Marschall, H.R., Korsakov, A.V., Luvizotto, G.L., Nasdala, L, Ludwig, T. (2009) On the occurrence and boron isotopic composition of tourmaline in (ultra)high-pressure metamorphic rocks. *Journal of the Geological Society* 166, 811–823.

McNeil, L.E., Grimsditch, M. (1993) Elastic-Moduli of Muscovite Mica. *Journal of Physics-Condensed Matter* 5, 1681–1690.

Melzer, S., Wunder, B. (2000) Island-arc basalt alkali ratios: Constraints from phengite-fluid partitioning experiments. *Geology* 28, 583–586.

Onuma, N., Higuchi, H., Wakita, H., Nagasawa, H. (1968) Trace element partitioning between two pyroxenes and the host lava. *Earth and Planetary Science Letters* 5, 47–51.

Rapp, J.F., Klemme, S., Butler, I.B., Harley, S.L. (2010) Extremely high solubility of rutile in chloride and fluoride-bearing metamorphic fluids: An experimental investigation. *Geology* 38, 323–326.

Scambelluri, M., Phillipot, P. (2001) Deep fluids in subduction zones, *Lithos* 55, 213–227.

Scambelluri, M., Bottazzi, P., Trommsdorff, V., Vannucci, R., Hermann, J., Gomez-Pugnaire, M.T., Sanchez-Vizcaino, V.L. (2001) Incompatible element-rich fluids released by antigorite breakdown in deeply subducted mantle. *Earth and Planetary Science Letters* 192, 457–470.

Selverstone, J., Franz, G., Thomas, S., Getty, S. (1992) Fluid variability in 2 GPa eclogites as an indicator of fluid behavior during subduction. *Contributions to Mineralogy and Petrology* 112, 341–357.

Shimizu, R., Ogasawara, Y. (2013) Diversity of potassium-bearing tourmalines in diamondiferous Kokchetav UHP metamorphic rocks: A geochemical recorder from peak to retrograde metamorphic stages. *Journal of Asian Earth Sciences* 63, 39–55.

Spandler, C., Hermann, J., Arculus, R., Mavrogenes, J. (2003) Redistribution of trace elements during prograde metamorphism from lawsonite blueschist to eclogite facies; implications for deep subduction-zone processes. *Contributions to Mineralogy and Petrology* 146, 205–222.

Spandler, C., Mavrogenes, J., Hermann, J. (2007) Experimental constraints on element mobility from subducted sediments using high-P synthetic fluid/melt inclusions. *Chemical Geology* 239, 228–249.

Syracuse, E.M., van Keken, P.E., Abers, G.A. (2010) The global range of subduction zone thermal models. *Physics of Earth and Planetary Interiors* 183, 73–90.

Tropper, P., Manning, C.E. (2007). The solubility of fluorite in H_2O and H_2O-NaCl at high pressure and temperature. *Chemical Geology* 242, 299–306.

Tropper, P., Manning, C.E., Essene, E.J. (2002). The substitution of Al and F in titanite at high pressure and temperature: Experimental constraints on phase relations and solid solution properties. *Journal of Petrology* 43, 1787–1814.

Tsay, A., Zajacz, Z., Ulmer, P., Sanchez-Valle, C. (2017) Mobility of major and trace elements in the eclogite-fluid system and element fluxes upon slab dehydration. *Geochimica et Cosmochimica Acta* 198, 70–91.

van Hinsberg, V.J., Schumacher, J.C. (2007a) Using estimated thermodynamic properties to model accessory phases: the case of tourmaline. *Journal of Metamorphic Geology* 25, 769–779.

van Hinsberg, V.J., Schumacher, J.C. (2007b) Intersector element partitioning in tourmaline: a potentially powerful single crystal thermometer. *Contributions to Mineralogy and Petrology* 153, 289–301.

van Hinsberg, V.J., Schumacher, J.C., Kearns, S., Mason, P.R.D., Franz, G. (2006) Hourglass sector zoning in metamorphic tourmaline and resultant major and trace-element fractionation. *American Mineralogist* 91, 717–728.

van Hinsberg, V.J., Migdisov, A.A., Williams-Jones, A.E. (2010) Reading the mineral record of fluid composition from element partitioning. *Geology* 38, 847–850.

van Hinsberg, V.J., Henry, D.J., Dutrow, B.L. (2011a) Tourmaline as a petrologic forensic mineral: A unique recorder of its geologic past. *Elements* 7, 327–332.

van Hinsberg, V.J., Henry, D.J., Marschall, H.R. (2011b) Tourmaline: an Ideal Indicator of Its Host Environment. *Canadian Mineralogist* 49, 1–16.

von Goerne, G., Franz, G., Heinrich, W. (2001) Synthesis of tourmaline solid solutions in the system Na_2O-MgO-Al_2O_3-SiO_2-B_2O_3-H_2O-HCl and the distribution of Na between tourmaline and fluid at 300 to 700 °C and 200 MPa. *Contributions to Mineralogy and Petrology* 141, 160–173.

Wilke, M., Schmidt, C., Dubrail, J., Appel, K., Borchert, M., Kvashnina, K., Manning, C.E. (2012) Zircon solubility and zirconium complexation in H_2O+Na_2O+SiO_2 ± Al_2O_3 fluids at high pressure and temperature. *Earth and Planetary Science Letters* 349, 15–25.

Wood, B.J., Blundy, J.D. (2003) Trace Element Partitioning under Crustal and Uppermost Mantle Conditions: The Influences of Ionic Radius, Cation Charge, Pressure, and Temperature. *Treatise on Geochemistry* 2, 395–424.

Xu, J., Kuang, Y., Zhang, B., Liu, Y., Fan, D., Li, X., Xie, H. (2016) Thermal equation of state of natural tourmaline at high pressure and temperature. *Physics and Chemistry of Minerals* 43, 315–326.

Zimmermann, R., Hammerschmidt, K., Franz, G. (1994) Eocene high pressure metamorphism in the Penninic units of the Tauern Window (Eastern Alps): evidence from ^{40}Ar-^{39}Ar dating and petrological investigations. *Contributions to Mineralogy and Petrology* 117, 175–186.